Electronic Supplementary Material (ESI) for Energy & Environmental Science

SUPPLEMENTARY INFORMATION for

Wiring Zinc in Three Dimensions Re-Writes Battery Performance—Dendrite-Free Cycling

Joseph F. Parker, Christopher N. Chervin, Eric S. Nelson, Debra R. Rolison,* and Jeffrey W. Long*

Surface Chemistry Branch – Code 6170
U. S. Naval Research Laboratory
Washington, DC 20375, USA

Table SI-1 Control experiments from twelve nearly identical (mass/volume) Zn electrodes. Each Zn sponge was treated using the electroreduction process described in the main text. The results demonstrate that the mass loss associated with the electroreduction step to convert a Zn@ZnO sponge to a Zn^0 sponge is remarkably reproducible.

Zn sponge number	Initial open-circuit potential (mV vs. Zn QRE)	Initial mass (g)	Final mass (g) *	Mass loss (%)
1	22.6	0.379	0.298	21.3
2	27.4	0.361	0.268	25.7
3	27.6	0.406	0.297	26.7
4	30.5	0.404	0.307	24.1
5	32.9	0.336	0.246	26.8
6	35.3	0.423	0.323	23.7
7	36.0	0.396	0.331	16.5
8	37.1	0.369	0.281	23.8
9	37.1	0.413	0.315	23.7
10	38.5	0.394	0.294	25.3
11	39.3	0.326	0.262	19.6
12	100.1	0.378	0.268	29.1
			AVERAGE MASS LOSS	23.9
			STD. DEVIATION	3.4

* Electroreduced Zn sponges were washed thoroughly with 18 MΩ cm water and dried in vacuo before reweighing.

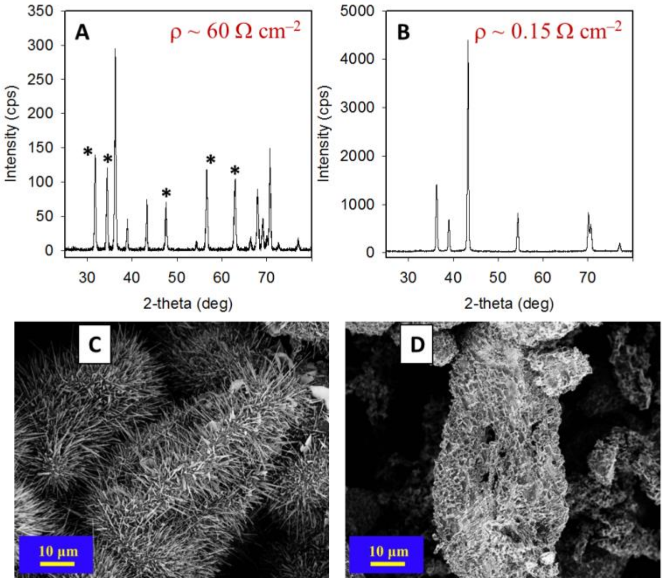

Fig. SI-1 Comparison of Zn sponges in (left) the as-prepared state and (right) after the electroreduction step. (A, B) X-ray diffraction demonstrating the loss of the ZnO content (∗) after reduction, with only reflections attributable to Zn metal remaining (Inset: values of real impedance, ρ, normalized to the 1.04-cm^2 geometric area of the sponge). (C, D) Scanning electron micrographs showing the removal of ZnO needles on the surface of the Zn walls in the sponge after electroreduction.

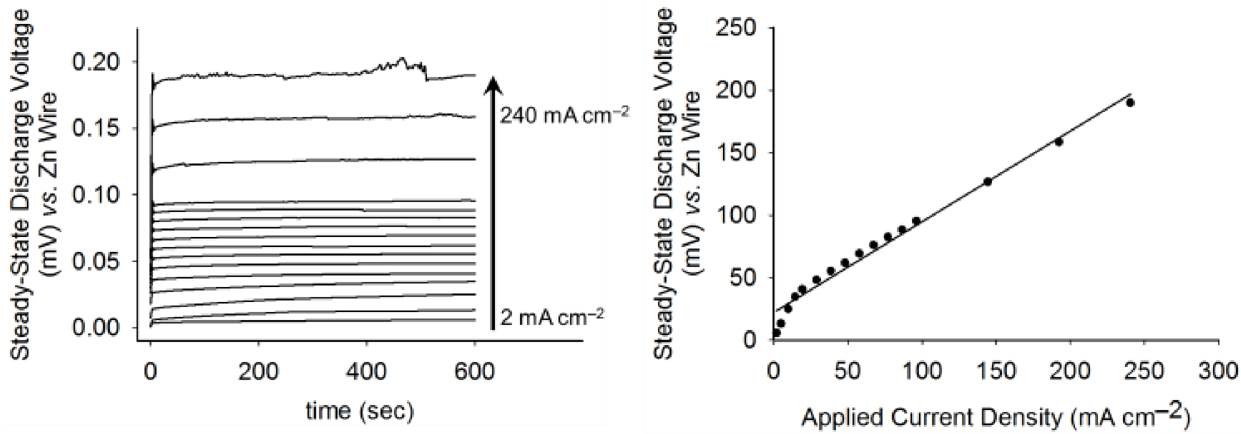

Fig. SI-2 (left) Steady-state discharge of a Zn sponge electrode in a flooded half-cell configuration in 6 M KOH with Zn wire quasi-reference and Pt-mesh counter electrodes. As applied current density is increased from 2–240 mA cm^{-2}, polarization remains < 200 mV and (right) scales linearly with applied load. The ability of the Zn sponge electrode to sustain such low polarization at very high current demands arises from the inherently fast electrode reaction (high exchange current density) for Zn^0/Zn^{2+} redox.

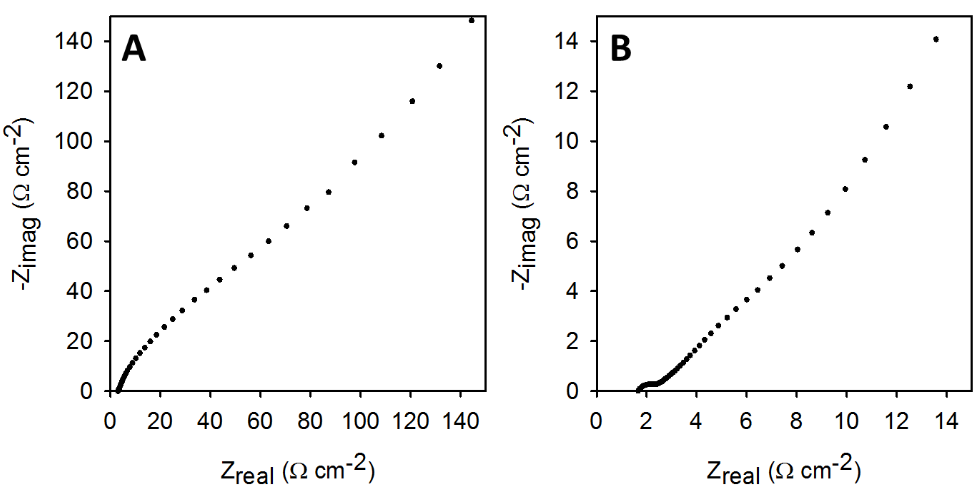

Fig. SI-3 Electrochemical impedance spectroscopy of a primary Zn–air full-cell (A) prior to discharge at 5 mA cm^{-2} to 83% DOD and (B) post-discharged. The air cathode used in this test is a composite of Vulcan carbon/cryptomelane/Teflon®. The low cell resistance (2–3 Ω cm^{-2}) in both cases confirms that, while the majority of the Zn has been oxidized to ZnO, the electrical conductivity characteristic of metallic Zn remains indicating that the Zn core of the ZnO-coated architecture is maintained after a deep discharge.

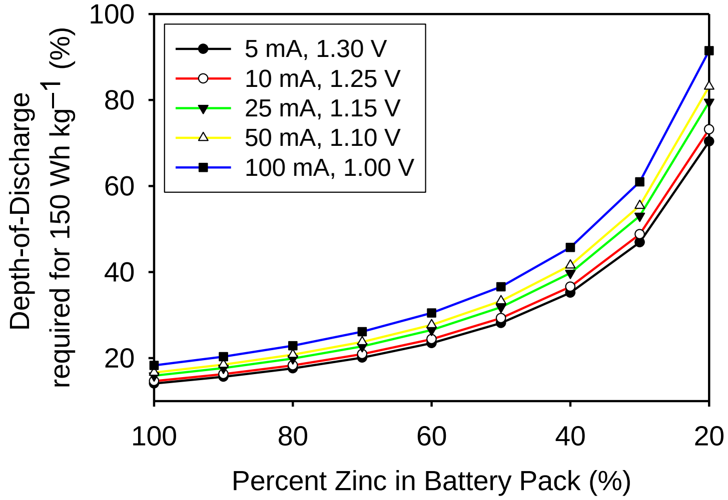

Fig. SI-4 Chart of depth-of-discharge (DOD) at Zn required to achieve 150 W h kg^{-1} (when projected into a Zn–air battery), a specific energy that rivals commercial Li-ion batteries, as a function of the Zn content of the battery pack at various loads (current demands). This analysis reveals that a fully engineered Zn–air battery, where Zn occupies 50–70% of the total pack mass would require 2–35% DOD at Zn.

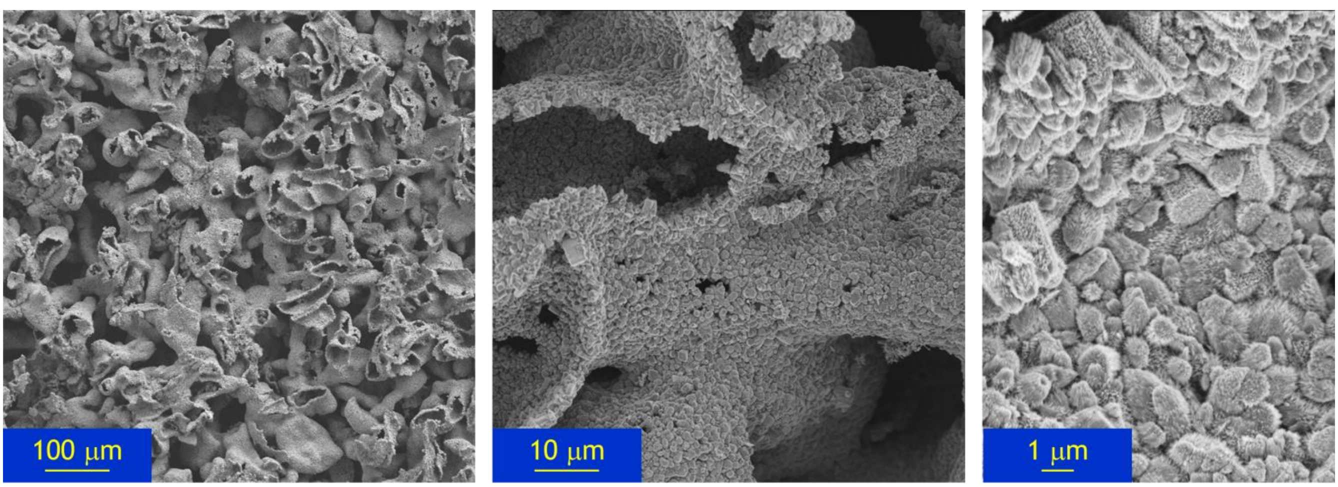

Fig. SI-5 Micrographs at various resolutions of the top (positive) Zn@ZnO sponge cycled at ±24 mA cm^{-2} for 43 scans (see Fig. 4 of main text for the cycling data and Fig. 5G–I for the opposing Zn@ZnO sponge micrographs). As a result of the differing masses of the two Zn@ZnO sponges in the model symmetrical cell, the top (positive) electrode was cycled to a lesser DOD (~9%) relative to the bottom (negative) electrode (~23%) presented in the main text. As expected, the morphology changes observed post-cycling are less pronounced in the top electrode because of the lower DOD. The deposition of compact Zn/ZnO products post-cycling occurs throughout the electrode structure and is consistent with uniformly distributed current density as a result of the well-wired sponge architecture, with no signs of dendrite formation. Note the revelation of the hollow character of the individual sintered Zn particles post-cycling.

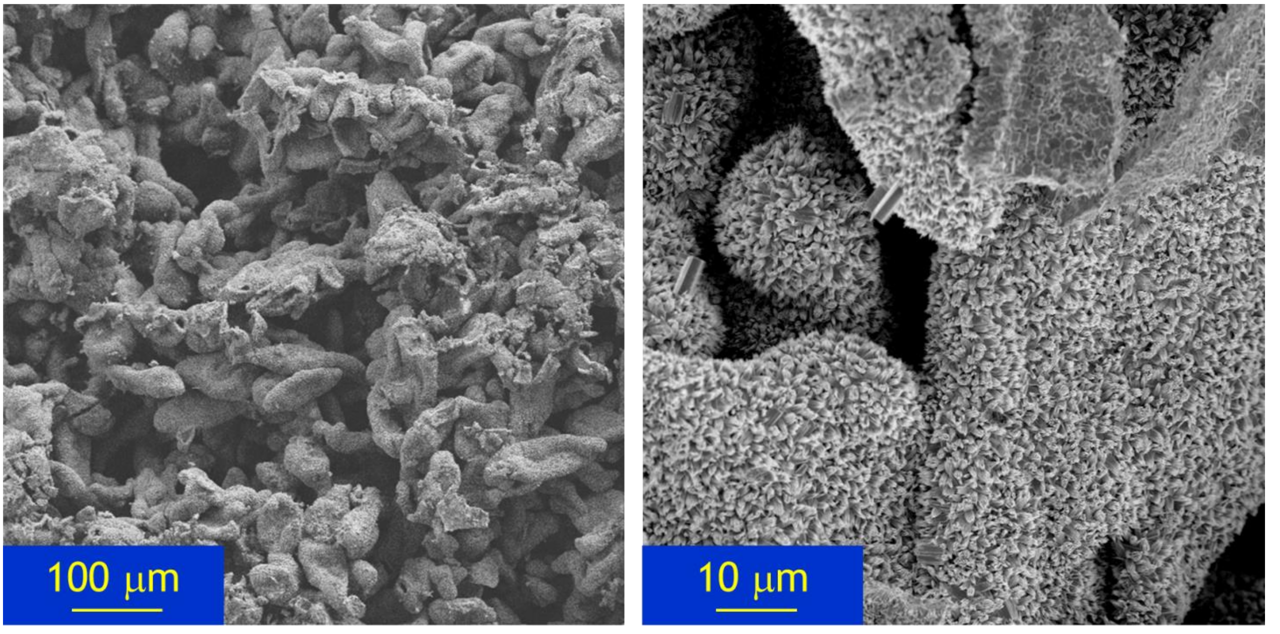

Fig. SI-6 Cross-sectional micrograph of a Zn@ZnO sponge cycled at ± 25 mA cm^{-2} to 5 % DOD for 25 scans (see Fig. 5D–F of main text). Approximately 1 mm of the separator-facing edge of the bottom electrode was removed with a razor and re-imaged. The deposition of sprout-like Zn/ZnO products post-cycling occurs throughout the electrode structure and is not limited to the surface of the Zn@ZnO sponge.

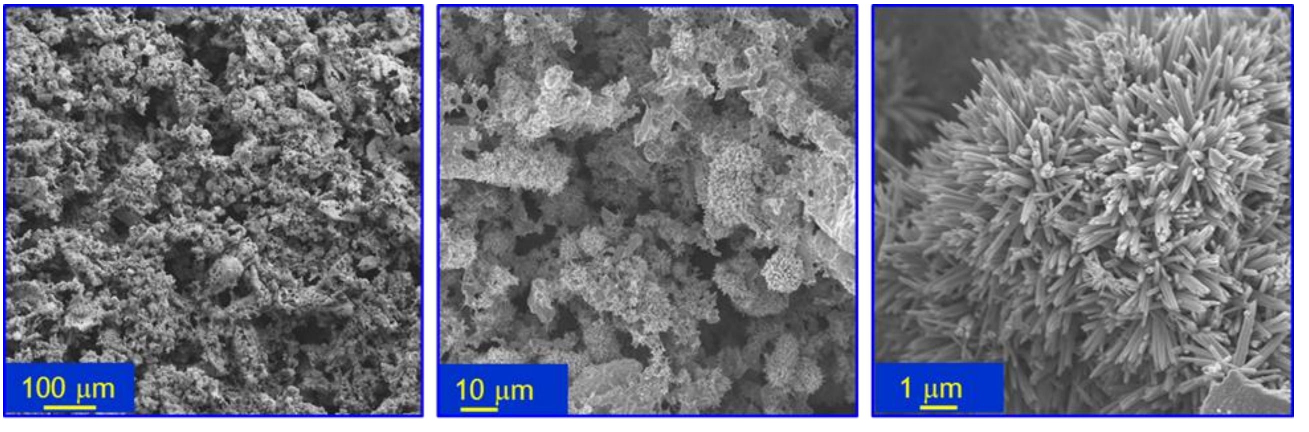

Fig. SI-7 Micrographs at various resolutions of the Zn sponge electrode cycled for 34 cycles in a Ag–Zn full cell at +5 mA cm^{-2} (discharge) and –3 mA cm^{-2} (charge)—see Fig. 6 of main text for the cycling data. As observed in the cycling data, the morphology observed after nearly a month of cycling reveals < 1 μm ZnO needles uniformly distributed throughout the electrode.

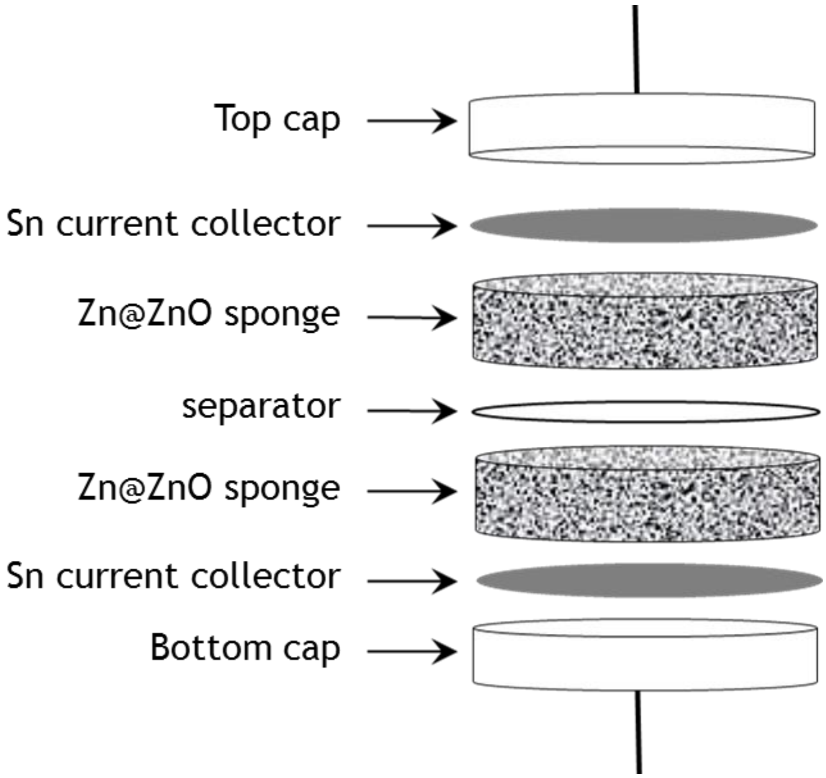

Fig. SI-8 Schematic of the Zn@ZnO symmetrical cell.